

## Experimental Research on Electrochemical Machining of an Arc-Shaped Slot Array

Feng Wang, Jianshe Zhao<sup>\*</sup>, Dingming Liu, Yantao Fan, Zongjun Tian

College of Mechanical and Electrical Engineering, Nanjing University of Aeronautics and Astronautics, Nanjing, 210016, China

\*E-mail: [zhaojs@nuaa.edu.cn](mailto:zhaojs@nuaa.edu.cn)

*Received:* 6 June 2018 / *Accepted:* 26 July 2018 / *Published:* 1 September 2018

---

Slot array structure is widely used in the aerospace industry, precision molds, instrumentation and other fields. Electrochemical machining has a unique advantage in the fabrication of slot arrays. However, there are still problems for electrochemical machining slot arrays with complex shapes, such as poor stability, low forming accuracy and difficult processing. To improve the processing ability of arc-shaped slot arrays, the influence of electrolyte flow pattern and pressure on flow field stability in a closed channel was studied with a computational fluid dynamics simulation, and the flow pattern and pressure parameters were optimized. Moreover, comparative experiments of continuous-feed electrochemical machining mode and low-frequency oscillation assisted electrochemical machining mode were carried out based on a self-developed oscillation apparatus. The influence of auxiliary oscillation motion on the processing stability frequency, average slot width, and slot slope was analyzed, and an arc-shaped slot array with a slot width of  $0.244\pm 0.01$  mm and high accuracy in shape and dimension was fabricated on a rotary workpiece.

---

**Keywords:** Arc-shaped slot array; Electrochemical machining; Low-frequency oscillation; Reverse flow; Computational fluid dynamics simulation

### 1. INTRODUCTION

Slot structure is extensively used in aerospace, electronic packaging, instrumentation, precision molds and other fields [1,2]. With the development of precision and intelligent industrial products, the requirements for slot structure machining accuracy and process stability have become stricter. Currently, frequently used slot machining technology includes mechanical cutting, electro-erosion machining, electrochemical machining, and laser beam machining [3-5]. Compared with other processing techniques, electrochemical machining has a unique advantage owing to the remarkable characteristics of no mechanical deformation, no thermal stress and no tool cathode loss [6,7].

However, there are still some problems with slot structure electrochemical machining, such as poor flow field stability, poor consistency for multiple-slots, and difficulty in machining complex-shaped slots.

For the purpose of improving the processing ability of slot structure electrochemical machining, some technical methods have been recently presented by scholars, such as auxiliary oscillation motion with continuous feed [8], high-speed rotation of the tool cathode [9], and improvement of the pulse power supply [10]. Liu et al. studied the flow field distributions in multi-slot electrochemical machining using the finite element method, and 30 slots were machined simultaneously by using the method of low-frequency vibration superimposed on the tool cathode continuous feed [11]. Qu et al. investigated the combined method of workpiece vibration and cathode traveling in wire electrochemical machining (WECM), and the transmissions of anodic products and hydrogen bubbles in the small inter-electrode gaps were significantly promoted by optimizing the vibration parameters. Moreover, groups of micro-slits with good consistency were successfully machined [12]. Xu et al. proposed the method of wire electrochemical machining with multiple cathodes, and micro-slit machining efficiency was significantly increased. Moreover, a variety of slit structures were successfully fabricated on a cobalt-based elastic alloy plate [13]. Liu et al. photographed the hydrogen bubble layer structures during the electrochemical machining process, and an inner annular groove with a width of 263  $\mu\text{m}$  and a depth of 340  $\mu\text{m}$  was machined with a high-speed rotating dentate cathode [14]. Ghoshal et al. investigated the distributions of current density in the small inter-electrode gap and conducted experimental research on the parameter optimization of pulse electrochemical machining. Finally, a micro-slot structure with smaller taper was fabricated using a micro-tool cathode [15]. However, previous research on slot structure electrochemical machining was concentrated overall on single slots and groups of linear slots, and there were few studies on the electrochemical machining of curved slots [16,17]. Currently, the fabrication of slots with complex shapes has brought great challenges to electrochemical machining technology.

In this work, the electrochemical machining of an arc-shaped slot array is taken as the research object, and the distributions of electrolyte flow velocity and pressure in a closed flow channel were investigated on the basis of a computational fluid dynamics (CFD) simulation. Furthermore, contrast experiments of continuous-feed electrochemical machining mode and low-frequency oscillation assisted electrochemical machining mode were carried out based on a self-developed electromagnetic driving oscillation apparatus, and the influence of auxiliary oscillation on the processing stability frequency, average slot width, and slot slope was investigated.

## **2. EXPERIMENTAL**

### *2.1. Determination of flow pattern and electrolyte pressure*

The electrolyte flow pattern in arc-shaped slot array electrochemical machining affects the fluid flow characteristics in the machining region and then directly affects the transmission of electrolytic products and the distribution of electrolytic conductivity. It can even determine whether the machining

process could be stably conducted. Moreover, previous studies have shown that compared with open flow field design, flow field fluctuation in the inter-electrode gap could be reduced significantly, and the processing stability could be improved by adopting a closed flow channel design [18,19]. Fig. 1 shows two types of closed flow channel structures with the same geometric configuration when the electrolyte flow patterns are forward and reverse flow. In view of the arc-shaped slot being centrally and symmetrically distributed with a rib width of only 0.1 mm, the influences of the tool cathode ribs on the closed flow channel structure are neglected, and the inter-electrode gap is set to 0.1 mm.

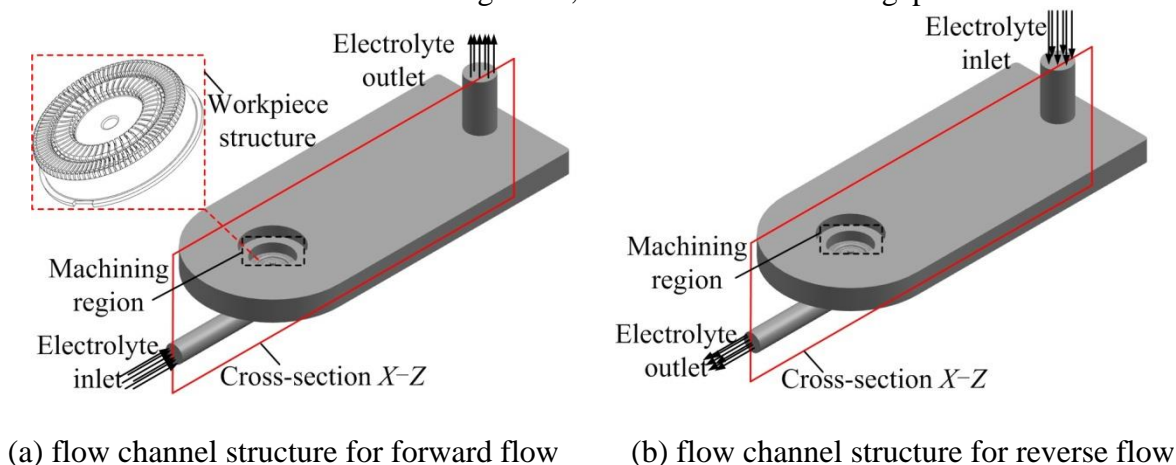
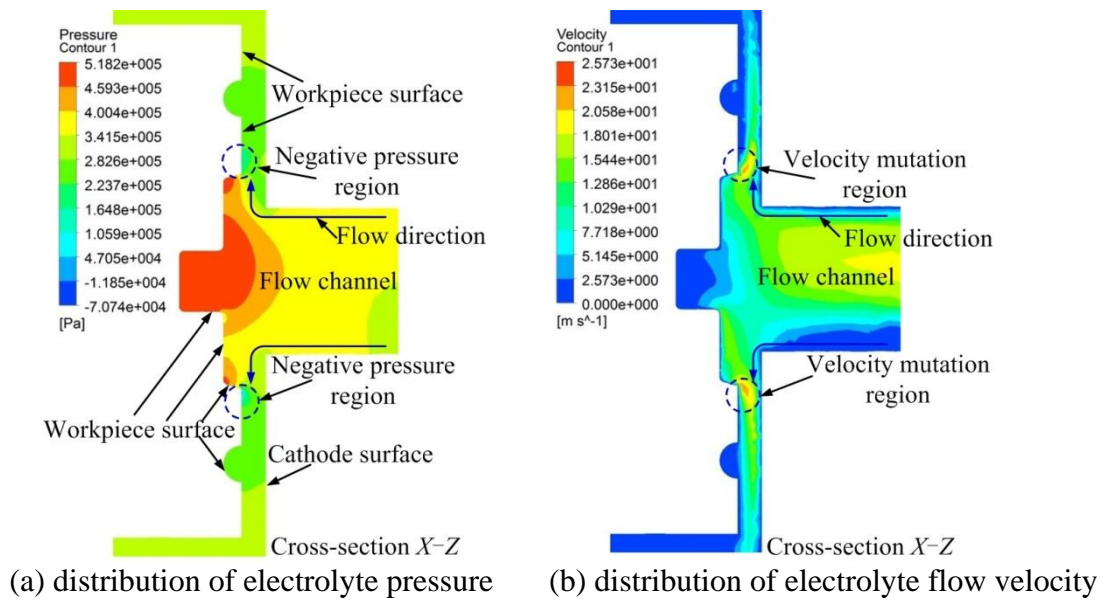


**Figure 1.** Closed flow channel structures for different electrolyte flow patterns

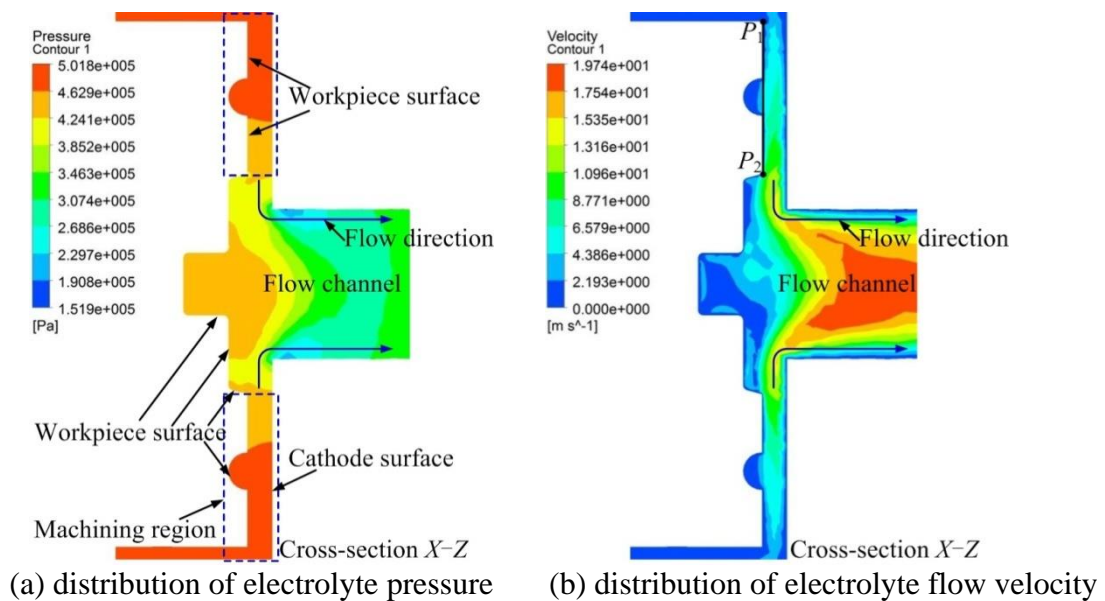
To analyze the effects of electrolyte flow pattern and pressure on flow field stability, the variations of electrolyte pressure and flow velocity in the closed flow channel are investigated with CFD simulation. The electrolyte temperature is set to 25 °C, and the dynamic viscosity coefficient  $\nu_T$  is set to  $0.9 \times 10^{-6} \text{ m}^2/\text{s}$ . The flow fields at the machining region, fluid inlet and fluid outlet are all assumed to be steadily distributed, and the electrolyte fluid is assumed to be as follows: (1) it is an ideal liquid that contains no hydrogen bubble, no oxygen bubbles and no sludge; (2) it is an incompressible constant Newtonian fluid; (3) temperature fluctuation and energy dissipation are both ignored. Therefore, the electrolyte fluid flow is restricted by the fluid state and basic conservation equations [20]. The flow field distribution in the closed flow channel is simulated based on the standard  $k-\epsilon$  turbulence model, and the effect of gravity on the steady flow of incompressible electrolyte fluid is not considered.

Fig. 2 shows the variations of pressure and flow velocity in the inter-electrode gap, when the flow pattern is forward, the electrolyte inlet pressure  $P_0$  is 0.5 MPa, and the electrolyte outlet pressure  $P_e$  is 0.3 MPa. As shown in Fig. 2(a), there is a significant negative pressure region in the inter-electrode gap near the inlet due to severe disturbance of the electrolyte fluid caused by the dramatic change of the workpiece geometric shape. In addition, the electrolyte pressure in the negative pressure region that is lower than the vaporization pressure is prone to produce the cavitation phenomenon and pressure alternation, which will seriously affect the flow field stability. As shown in Fig. 2(b), due to the sharp decrease in flow channel cross-sectional area from the inlet to the machining region, the electrolyte flow velocity near the inlet increases rapidly and fluctuates violently. The kinetic energy of the electrolyte fluid also increases dramatically. However, because the variation of the flow channel

cross-sectional area in the inter-electrode gap tends to be gentle, the flow velocity uniformly decreases from 25 m/s to 7 m/s along the electrolyte flow direction.



**Figure 2.** Flow field distribution in the inter-electrode gap for forward flow



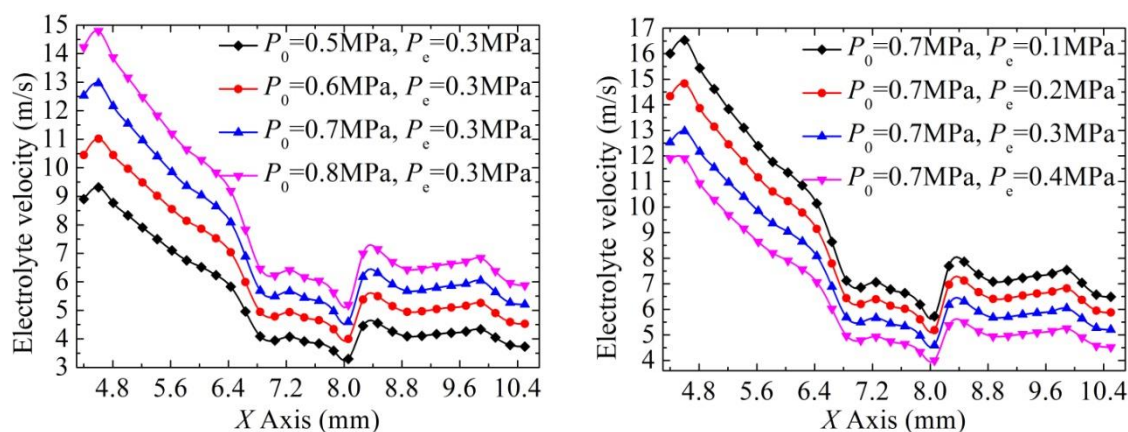
**Figure 3.** Flow field distribution in the inter-electrode gap for reverse flow

Fig. 3 shows the variations of pressure and flow velocity in the inter-electrode gap for reverse flow, with inlet pressure  $P_0$  of 0.5 MPa and the outlet pressure  $P_e$  of 0.3 MPa. The electrolyte pressure is uniformly reduced from 0.5 MPa to 0.42 MPa along the electrolyte flow direction, and the pressure fluctuation is slight, as shown in Fig. 3(a). Moreover, there are no negative pressure and pressure alternating regions in the inter-electrode gap. The flow velocity in the machining region increases uniformly from 4 m/s to 13 m/s along the electrolyte flow direction, and the flow velocity fluctuation

is relatively gentle, as shown in Fig. 3(b). Furthermore, there is no velocity mutation region in the machined surface, and the flow field distribution tends to be stable.

The simulation of different electrolyte flow patterns shows that compared with forward flow, reverse flow adapts well to the changes of flow channel cross-section and workpiece surface profile. There is no negative pressure region, no pressure alternating region, and no velocity mutation region in the inter-electrode gap, and the reverse flow field distribution is relatively stable. Moreover, flow velocity and pressure fluctuations in the inter-electrode gap are small, and the uniformity of flow field distribution for reverse flow is also good. Therefore, the reverse flow pattern is more suitable for the experiments on arc-shaped slot array electrochemical machining.

The inlet pressure  $P_0$  provides the velocity energy of fluid flowing in the flow channel. Previous studies have shown that in order to achieve a turbulent electrolyte flow state, conduct normal electrochemical reactions, inhibit the electrolyte temperature rise and exhaust electrolytic products in a timely manner, the electrolyte flow velocity should be more than 5 m/s. By increasing the outlet pressure  $P_c$ , the electrolyte pressure difference between the inlet and outlet could be reduced, and the pressure mutation in the flow channel could also be reduced. Fig. 4 shows the velocity distributions of section line  $P_1P_2$  under different inlet and outlet pressure parameters. The section line  $P_1P_2$  is consistent with the machining region of the slot array on the workpiece, and the electrolyte flow pattern is reverse flow. It is known from Fig. 4(a) that when the outlet pressure is fixed, the electrolyte flow velocity increases gradually with the inlet pressure, but variations of section line electrolyte flow velocity are similar. It is known from Fig. 4(b) that when the inlet pressure is fixed, the electrolyte flow velocity decreases gradually with the increase of outlet pressure, and the fluctuation decreases accordingly.



(a) flow velocity with different inlet pressure (b) flow velocity with different outlet pressure

**Figure 4.** Distribution of flow velocity for section line  $P_1P_2$  with varied electrolyte pressure

Flow field simulation analyses with different inlet and outlet pressure parameters show that increasing the inlet and reducing the outlet pressure is conducive to improving the machining region flow velocity, and then the exhaustion of electrolytic products and inhibition of the temperature rise are facilitated. However, high inlet pressure has higher requirements for the electrolyte pipeline and pump, and the overly low outlet pressure is not conducive to the uniform removal of anode material

due to the sharp fluctuation of flow velocity. When the inlet pressure  $P_0$  is 0.7 MPa and the outlet pressure  $P_e$  is 0.2 MPa, the machining region electrolyte flow velocity varies from 5 m/s to 15 m/s. The flow velocity is relatively high and the fluctuation is slight.

## 2.2. Apparatus for slot array electrochemical machining

The CFD simulation results show that the flow field mutation in the inter-electrode gap can be avoided, and the electrolyte flow velocity can be improved by adopting the reverse flow pattern with reasonable inlet and outlet pressure parameters, but it is still difficult to change the electrolyte flow velocity distribution in the machining region. During the process of continuous-feed electrochemical machining of arc-shaped slot arrays, due to the increase of pressure loss along the flow direction with the increment of machining depth, the effect of electrolyte renewal on the slot bottom is significantly weakened, and anodic products, gaseous products and Joule heat easily accumulate in the low-velocity region. Thus, the improvement of processing stability is restricted. Previous research has shown that when low-frequency oscillation is superimposed on a continuous feed, problems of electrolytic product removal and electrolyte renewal in the low-velocity region can be resolved by periodic change of the inter-electrode gap [21].

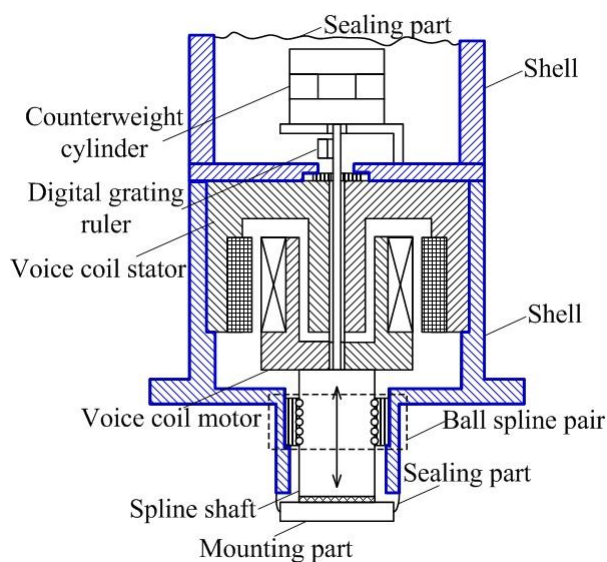


**Figure 5.** Schematic diagram of the oscillation apparatus

For the purpose of improving the processing stability and forming accuracy of the arc-shaped slot array, comparative experiments of continuous-feed electrochemical machining mode and low-frequency oscillation assisted electrochemical machining mode were conducted, and low-frequency vertical oscillation was superimposed on the continuous feed in the low-frequency oscillation assisted electrochemical machining mode. Fig. 5 shows the structure of the self-developed low-frequency oscillation apparatus, and Fig. 6 shows the experimental apparatus for the electrochemical machining of arc-shaped slot arrays. The oscillation apparatus includes the voice coil motor, voice coil stator, ball spline, digital grating ruler, counterweight cylinder and shell. The linear voice coil motor is a driving component of the oscillation apparatus, the ball spline pair is a motion guiding component, and the

digital grating ruler is an element of oscillation position detection and feedback. The Elmo Cello intelligent servo controller is used to accurately control the position of the voice coil motor, and then high precision oscillation motion is realized. Moreover, protections for voice coil motor overload, undervoltage and short circuits are realized. The performance parameters of the oscillation apparatus are as follows: the maximum load weight is 9 kg, the peak thrust is 4715.2 N, the continuous thrust is 1111.4 N, the oscillation frequency is arbitrarily adjustable within the range of 0 to 50 Hz, the amplitude is arbitrarily adjustable within the range of 0 to 1 mm, the output oscillation waveform is a sine wave or a trapezoidal wave, the maximum oscillation waveform tracking error can be controlled within the range of 0.01 mm and the repeatable positioning accuracy can be controlled within 3  $\mu\text{m}$ .

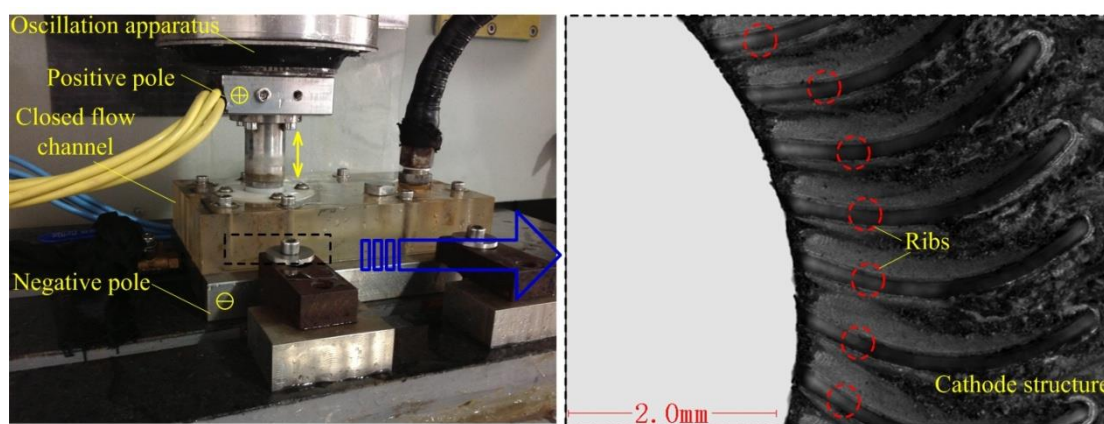


**Figure 6.** Experimental apparatus and cathode structure for slot array electrochemical machining

### 2.3. Experimental arrangements

For the purpose of analyzing the effect of continuous-feed electrochemical machining mode and low-frequency oscillation assisted electrochemical machining mode on the processing ability of arc-shaped slot arrays, comparative experiments with different amplitudes and oscillation frequencies were carried out, and changes to the processing stability frequency, average slot width, and slot slope under different oscillation motions were studied. The main machining parameters are shown in Table 1, and the initial inter-electrode gap distribution for different amplitudes is shown in Fig. 7. The dimension detection of the arc-shaped slot array is shown in Fig. 8. A digital microscope was used to detect the entrance slot width  $D_1$ , the middle slot width  $D_2$ , and the bottom slot width  $D_3$  of the workpiece at four different positions. The average slot width  $D_a$  and slot slope  $\delta$  of each detection position are calculated by equations (1) and (2), respectively, and  $h$  is the workpiece thickness.

$$D_a = (D_1 + D_2 + D_3)/3 \quad (1)$$

$$\delta = (D_1 - D_3)/2h \quad (2)$$

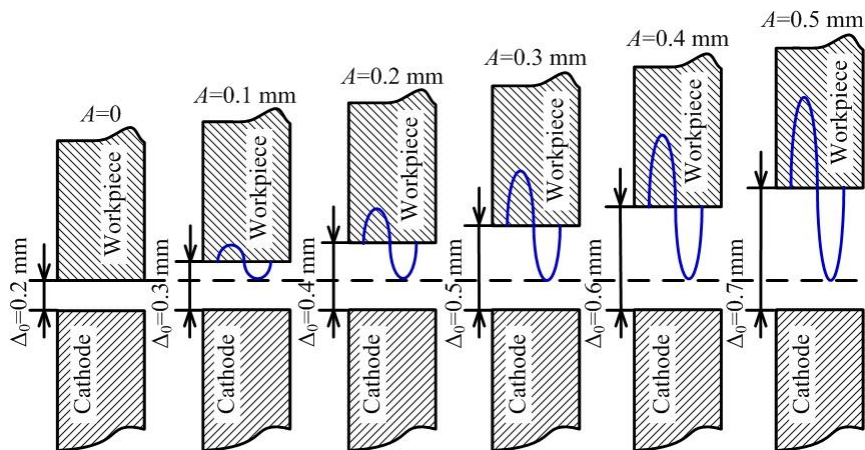


Figure 7. Initial inter-electrode gaps for different oscillation amplitudes

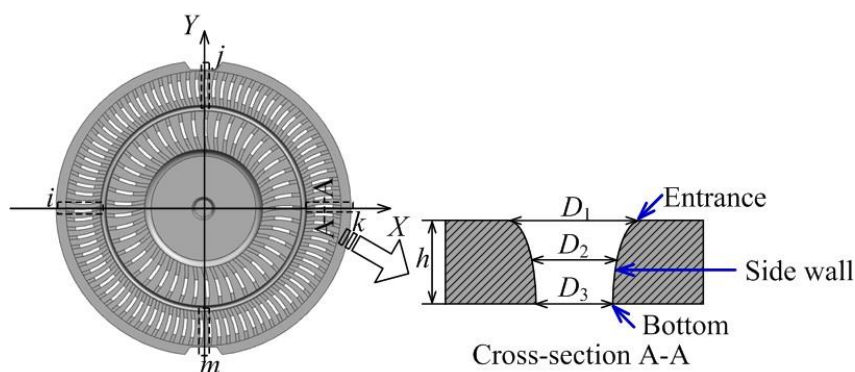


Figure 8. Schematic diagram for the detection of arc-shaped slot arrays

Table 1. Main parameters of arc-shaped slot array electrochemical machining

| Machining parameter                         | Value                        |
|---|------------------------------|
| Workpiece material                          | SS304                        |
| Cathode material                            | Beryllium bronze             |
| Initial inter-electrode gap $\Delta_0$ (mm) | 0.2, 0.3, 0.4, 0.5, 0.6, 0.7 |
| Peak voltage $U$ (V)                        | 8, 10                        |
| Impulse frequency (kHz)                     | 3                            |
| Duty ratio                                  | 0.6                          |
| Electrolyte composition                     | $\text{NaNO}_3$              |
| Electrolytic conductivity $\kappa$ (S/m)    | 7.9                          |
| Flow pattern                                | Reverse flow                 |
| Inlet pressure $P_0$ (MPa)                  | 0.7                          |
| Outlet pressure $P_e$ (MPa)                 | 0.2                          |
| Continuous feed rate (mm/min)               | 0.25                         |
| Amplitude $A$ (mm)                          | 0, 0.1, 0.2, 0.3, 0.4, 0.5   |
| Oscillation frequency $f$ (Hz)              | 0, 10, 20, 30, 40, 50        |
| Workpiece thickness (mm)                    | 0.5                          |

### 3. RESULTS AND DISCUSSION

#### 3.1. Effect of auxiliary oscillation on process stability

To investigate the effect of auxiliary oscillation motion on the processing stability of arc-shaped slot array electrochemical machining, comparative experiments with different amplitudes and oscillation frequencies were carried out. The peak voltage was set to 10 V and the continuous feed rate was set to 0.25 mm/min. The oscillation parameters for each group were repeated 15 times. The processing stability frequencies for varied oscillation frequencies are shown in Fig. 9(a), and the processing stability frequencies for varied amplitudes are shown in Fig. 9(b).

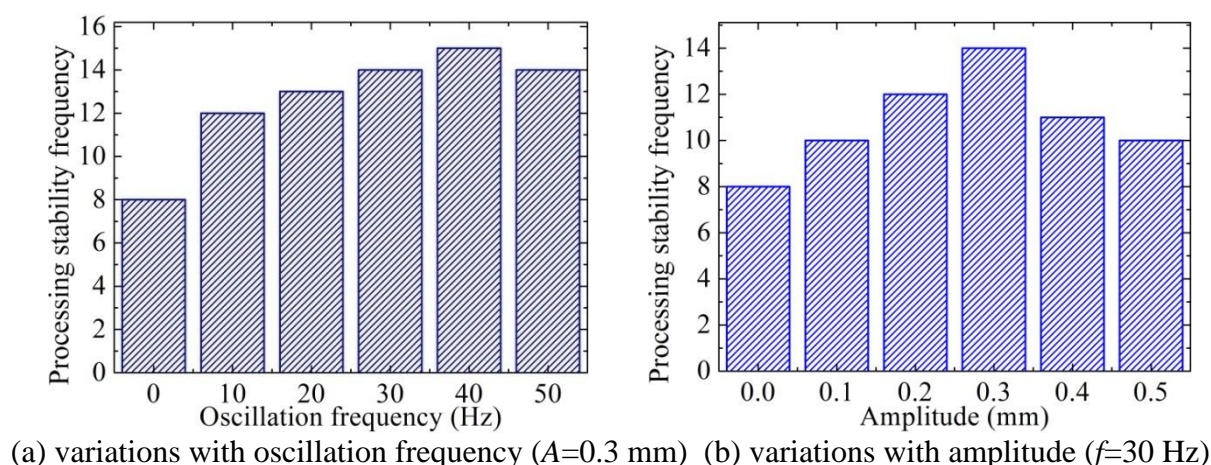


**Figure 9.** Processing stability frequencies for different oscillation motions

It is known from Fig. 9 that compared with the continuous-feed electrochemical machining mode ( $A=0$  mm or  $f=0$  Hz), the low-frequency oscillation assisted electrochemical machining mode can significantly improve the processing stability of slot array electrochemical machining. When the oscillation frequency or amplitude is low, there is still a significant low velocity region in the inter-electrode gap, resulting in the accumulation of gaseous products and the cathode rib is easy to be deformed due to the surface tension of hydrogen bubbles [22]. Therefore, the processing stability frequency is relatively low. When the amplitude is set to 0.3 mm, the processing stability frequency generally increases with the increment of the oscillation frequency. The processing stability frequency increases significantly when the oscillation frequency increases from 0 to 30 Hz. When the oscillation frequency is higher than 30 Hz, the processing stability frequency changes little. When the oscillation frequency is set to 30 Hz, the processing stability frequency increases at first and then decreases with increasing amplitude. As the amplitude increases from 0 to 0.3 mm, the processing stability frequency increases gradually. However, the processing stability decreases significantly when the amplitude is greater than 0.3 mm. The amplitude increase is conducive to enhancing the electrolyte scouring effect on cathode bottom surface, thereby facilitating the exclusion of gaseous products [23]. However, in the meantime, the electrolyte impedance between the workpiece and the tool cathode increases significantly with increasing amplitude, and then the electrochemical dissolution rate at the slot bottom

decreases significantly, and it is likely to produce spark discharging, or even a short circuit when the feed rate is greater than the electrochemical dissolution rate at the bottom. Thus, the processing stability frequency decreases with the increment of amplitude in the range of 0.3 mm to 0.5 mm.

The typical current curves of the slot array electrochemical machining process collected by Hall current sensor are shown in Fig. 10. When the continuous-feed electrochemical machining mode is adopted, the inter-electrode gap changes dramatically with the ribs of the tool cathode gradually entering the interior of the workpiece (feeding distance is close to 0.2 mm), and then significant fluctuations are produced in the machining current curves. Moreover, when the feeding distance is close to 0.6 mm, the frontal inter-electrode gap changes dramatically, and the flow velocity distribution also changes sharply due to the gradual penetration of the slot array bottom. Thus, the current curve fluctuation is aggravated. In the process of low-frequency oscillation assisted electrochemical machining, the current curve fluctuation is more stable, and the process stability is better when the amplitude is 0.3 mm and the oscillation frequencies are 30 Hz and 50 Hz. However, when the oscillation frequency is 30 Hz and the amplitude is increased to 0.5 mm, as the residence times of the cathode ribs inside the workpiece are sharply reduced, the electrochemical dissolution rates at the slot array bottom are significantly reduced. Moreover, the excessive amplitude leads to the enhancement of electrolyte pumping action, and resulting in a separation between the cathode and the electrolyte surface [24]. Thus, the current curve fluctuation is large, and the process stability is poor at the initial processing and slot array penetration stages.

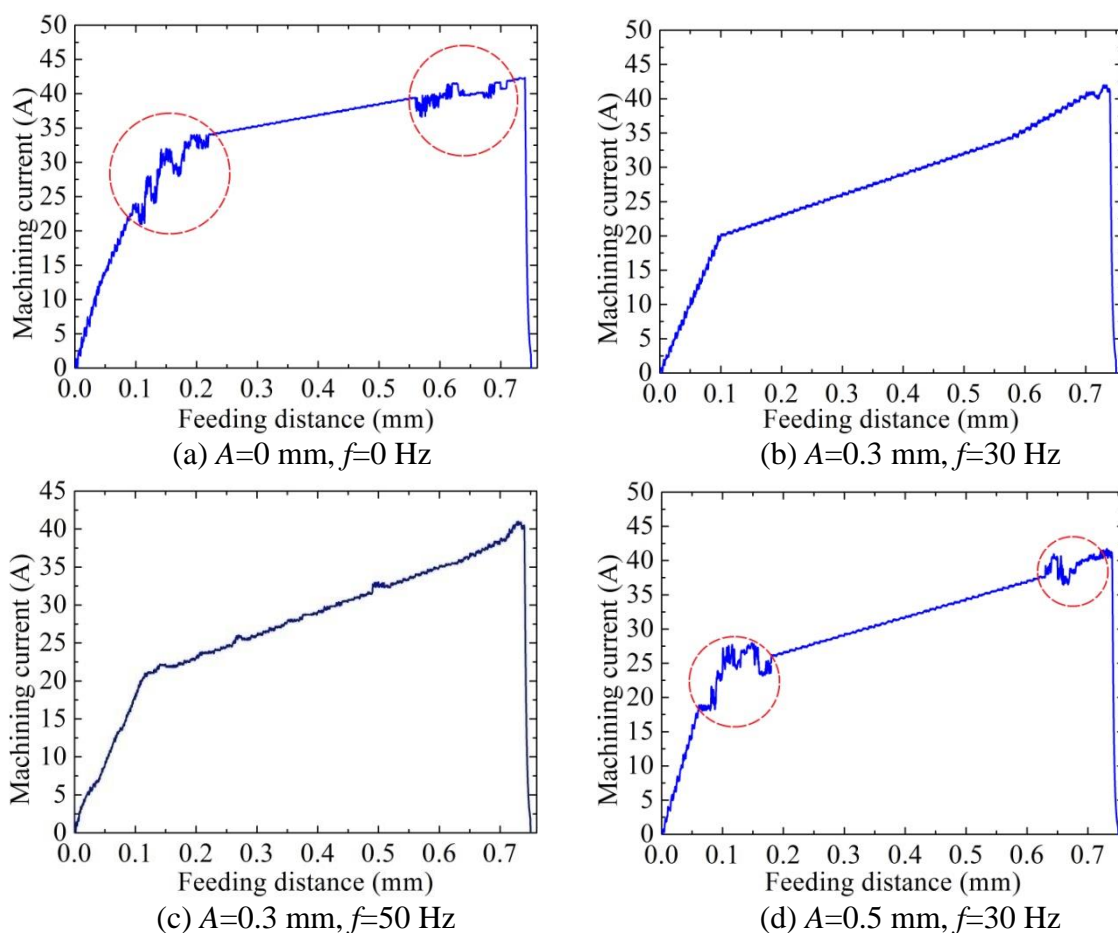


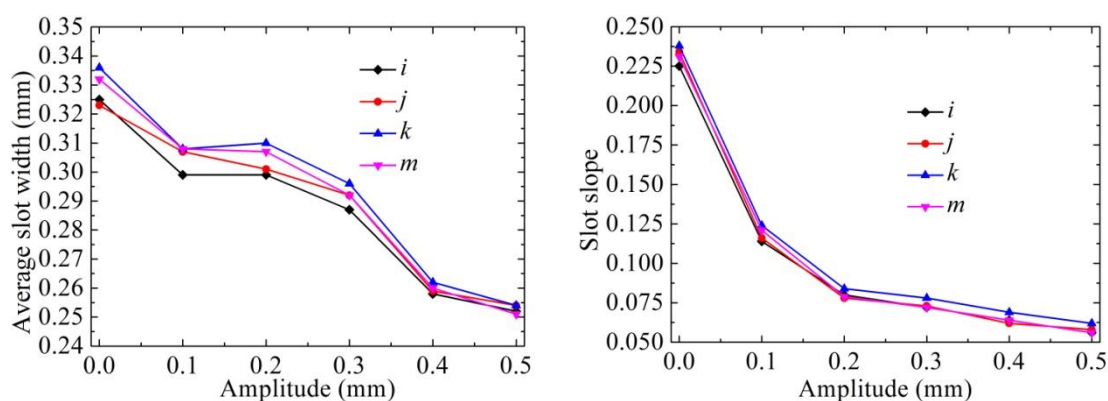
**Figure 10.** Typical current curves collected by using different electrochemical machining modes  
3.2. Effect of auxiliary oscillation on accuracy

To investigate the influence of auxiliary oscillations on the forming accuracy of arc-shaped slot arrays, contrast experiments with different oscillation parameters were conducted. The peak voltage was set to 10 V and the continuous feed rate was set to 0.25 mm/min. Moreover, detection and analysis of slot width and slot slope at different workpiece positions was also conducted.

### 3.2.1. Effect of amplitude on accuracy

The variations of average slot width and slope at different detection positions under different amplitudes are shown in Fig. 11. It is known from Fig. 11(a) that the average slot width of each detection position generally decreases with the increment of amplitude, but the average slot width changes little with increasing amplitude when it is less than 0.2 mm. The average slot width gradually decreases and tends to be consistent when the amplitude is greater than 0.3 mm. The slot slope of each detection position decreases significantly with the increment of amplitude, as shown in Fig. 11(b). However, the slot slope varies slightly with increasing amplitude when it is greater than 0.2 mm.

It is known from the average slot width and slope for different amplitudes that when it is less than 0.2 mm, the influence of oscillation motion on the average slot width is not significant because the amplitude is significantly smaller than the workpiece thickness. The residence times of cathode ribs staying outside the workpiece extend with the increasing amplitude, resulting in a significant increase in the electrolyte impedance in the inter-electrode gap and a significant decrease in the electrochemical dissolution rate. Thus, the average slot width decreases significantly. Moreover, electrolyte convection is further strengthened with the increment of amplitude, which promotes the removal of sludge and gaseous products in the low velocity region, and then the electrochemical dissolution rate of the anode material tends to be stable [25]. Therefore, the slot slope decreases significantly, and the average slot width of each detection position tends to be the same.

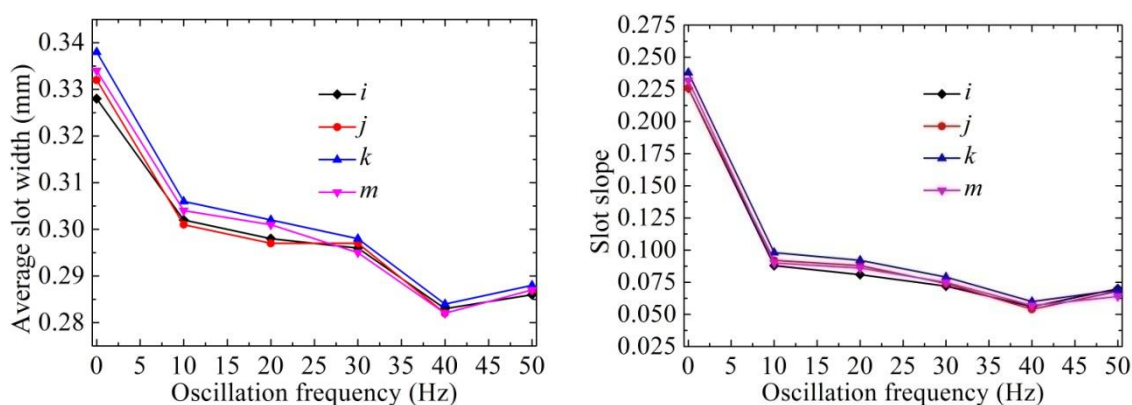


(a) change of slot width with amplitude ( $f=30$  Hz) (b) change of slope with amplitude ( $f=30$  Hz)

**Figure 11.** Variations of the average slot width and slot slope with amplitude

### 3.2.2. Effect of oscillation frequency on accuracy

The variations of average slot width and slope at different positions under different oscillation frequencies are shown in Fig. 12. As depicted in Fig. 12(a), the average slot width of each position generally decreases with increasing oscillation frequency, but it increases with increasing oscillation frequency higher than 40 Hz. Moreover, the average slot width of each detection position is quite different when the oscillation frequency is low, but tends to be the same with the increment of oscillation frequency. As depicted in Fig. 12(b), the slot slope of each detection position decreases generally with increasing oscillation frequency, and the slot slope of low-frequency oscillation assisted electrochemical machining mode is less than 25% of the continuous-feed electrochemical machining mode when the oscillation frequency is higher than 30 Hz. Moreover, the slot slope of each detection position also tends to be the same with the increasing oscillation frequency.



(a) change of slot width with frequency ( $A=0.3$  mm) (b) change of slope with frequency ( $A=0.3$  mm)

**Figure 12.** Variations of the average slot width and slope with oscillation frequency

It can be concluded from the average slot width and slope for different oscillation frequencies that increasing oscillation frequency is beneficial to the timely exclusion of gaseous products, sludge and Joule heat in the low velocity region, and the uniformity of electrolytic conductivity is enhanced. Furthermore, the slot-array slope could be reduced, and the uniformity of slot width at each detection position could be improved. However, the electrolytic products at the slot bottom have not been excluded in a timely manner and are dragged into the inter-electrode gap due to the excessively short period when the oscillation frequency is higher than 40 Hz, and this is not conducive to increasing the electrochemical dissolution rate at the slot bottom. However, the electrochemical dissolution rate at the slot entrance still increases significantly because of further electrolyte convection enhancement with increasing oscillation frequency. Thus, the average slot width and slope increase when the oscillation frequency is higher than 40 Hz. Moreover, Wang et al. found that the tool cathode is prone to vibrate with electrolyte scouring when the oscillation frequency is relatively high [26]. Therefore, when the oscillation frequency is higher than 40 Hz, the small elastic deformations of the tool cathode ribs are

easy to produce due to the strong disturbance of the high electrolyte flow velocity, and then the average slot width and slope can also be increased.

### 3.3. Fabrication of arc-shaped slot arrays

Fabrication of arc-shaped slot arrays was carried out by optimizing the machining parameters on the basis of the effect of different oscillation motions on processing stability and forming accuracy of the slot array electrochemical machining. The peak voltage was set to 8 V, the oscillation frequency was set to 30 Hz, the amplitude was set to 0.3 mm, and the continuous feed rate was set to 0.25 mm/min. As shown in Fig. 13, arc-shaped slot arrays are fabricated in the inner and outer rings of the rotary workpieces, and the machining processes are all relatively stable. Moreover, the slot width at the entrance can be controlled within the range of  $0.244 \pm 0.01$  mm, the slot slope can be controlled in the range of 0.045 to 0.052, and the arc radius of the slot array can be controlled within the range of R 2.45 mm to R 2.55 mm. Altogether, the shape and dimensions of the arc-shaped slot array are highly accurate.

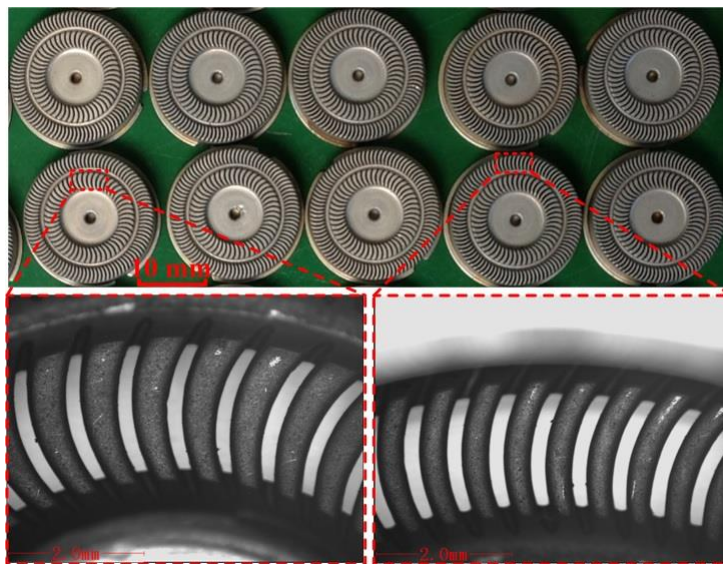


**Figure 13.** Fabrication of arc-shaped slot arrays with optimized parameters ( $A=0.3$  mm,  $f=30$  Hz)

## 4. CONCLUSIONS

This paper focuses on the electrochemical machining of arc-shaped slot arrays. The influences of electrolyte flow pattern and pressure on the flow field distribution in a closed flow channel were studied with CFD simulation. Moreover, contrast experiments of continuous-feed electrochemical machining mode and low-frequency oscillation assisted electrochemical machining mode were carried out. Several conclusions are reached through this research:

(1) Compared with electrolyte forward flow, there were no negative pressure and pressure alternating regions in the inter-electrode gap by adopting the electrolyte reverse flow pattern, and the

fluctuation of electrolyte flow velocity was relatively stable. Increasing electrolyte inlet pressure and reducing the outlet pressure increased the electrolyte flow velocity in the machining region, but it was still difficult to change.

(2) Compared with continuous-feed electrochemical machining mode, low-frequency oscillation assisted electrochemical machining mode significantly improved the stability of arc-shaped slot array electrochemical machining. The processing stability frequency generally increased with the increment of oscillation frequency when the amplitude was fixed, and the processing stability frequency increased at first and then decreased with the increment of amplitude when the oscillation frequency was fixed. Furthermore, processing stability was relatively stable when the amplitude was 0.3 mm and the oscillation frequency was in the range of 30 Hz to 50 Hz.

(3) The average slot width and slope generally decreased with increasing amplitude and oscillation frequency, and the uniformity of slot width increased at each detection position. However, the average slot width and slope increased when the oscillation frequency was overly high.

#### ACKNOWLEDGEMENTS

The authors would like to acknowledge the financial support provided by the Fundamental Research Funds for the Central Universities (3082018NF2018006) and Funding for Outstanding Doctoral Dissertation in NUAA (BCXJ16-05).

#### References

1. D. Deng, Y. Tang, J. Zeng, S. Yang and H. Shao, *Int. J. Heat. Mass. Trans.*, 77 (2014) 311.
2. K. K. Saxena, J. Qian and D. Reynaerts, *Int. J. Mach. Tool. Manuf.*, 127 (2018) 28.
3. G. D. Kim and B. G. Loh, *J. Mater. Process. Technol.*, 190 (2007) 181.
4. J. Yan, T. Kaneko, K. Uchida, N. Yoshihara and T. Kuriyagawa, *Int. J. Adv. Manuf. Technol.*, 50 (2010) 991.
5. A. Moroki, R. Kitano, M. Obara and H. Tsuda, *Jpn. J. Appl. Phys.*, 44 (2005) 8753.
6. H. S. J. Altena, *J. Mater. Process. Technol.*, 149 (2004) 18.
7. K. P. Rajurkar, M. M. Sundaram and A. P. Malshe, *Procedia. CIRP.*, 6 (2013) 13.
8. F. Wang, J. S. Zhao, X. L. Zhang, Z. W. Yang, W. M. Gan and Z. J. Tian, *Int. J. Adv. Manuf. Technol.*, 90 (2016) 971.
9. X. L. Fang, P. F. Zhang, Y. B. Zeng, N. S. Qu and D. Zhu, *J. Mater. Process. Technol.*, 227 (2016) 129.
10. V. Rathod, B. Doloi and B. Bhattacharyya, *Int. J. Adv. Manuf. Technol.*, 76 (2015) 51.
11. J. Liu, X. C. Jiang and D. Zhu, *Procedia. CIRP.*, 42 (2016) 799.
12. N. S. Qu, K. Xu, Y. B. Zeng and Q. Yu, *Int. J. Electrochem. Sci.*, 8 (2013) 12163.
13. K. Xu, Y. B. Zeng, P. Li, X. L. Fang and D. Zhu, *Int. J. Electrochem. Sci.*, 11 (2016) 5403.
14. G. X. Liu, Y. J. Zhang, S. Z. Jiang, J. W. Liu, G. K. Gyimah and H. P. Luo, *Int. J. Mach. Tool. Manuf.*, 102 (2016) 22.
15. B. Ghoshal and B. Bhattacharyya, *Int. J. Adv. Manuf. Technol.*, 76 (2015) 39.
16. A. K. M. D. Silva, H. S. J. Altena and J. A. McGeough, *CIRP. Ann-Manuf. Technol.*, 52 (2003) 165.
17. A. K. M. D. Silva, H. S. J. Altena and J. A. McGeough, *CIRP. Ann-Manuf. Technol.*, 49 (2000) 151.
18. D. Zhu, J. C. Zhang, K. L. Zhang, J. Liu, Z. Chen and N. S. Qu, *Int. J. Adv. Manuf. Technol.*, 80 (2015) 637.
19. J. S. Zhao, X. L. Zhang, Z. W. Yang, Y. M. Lü and Y. F. He, *Int. J. Adv. Manuf. Technol.*, 91 (2017)

147.

20. L. Dabrowski and T. Paczkowski, *Russ. J. Electrochem.*, 41 (2005) 91.
21. I. Yang, M. S. Park and C. N. Chu, *Int. J. Precis. Eng. Manuf.*, 10 (2009) 5.
22. Y. B. Zeng, Y. Qia, S. H. Wang and D. Zhu, *CIRP. Ann-Manuf. Technol.*, 61 (2012) 195.
23. X. L. Fang, X. H. Zou, M. Chen and D. Zhu, *CIRP. Ann-Manuf. Technol.*, 66 (2017) 205.
24. M. S. Hewidy, S. J. Ebeid, T. A. El-Taweel and A. H. Youssef, *J. Mater. Process. Technol.*, 189 (2007) 466.
25. K. Xu, Y. B. Zeng, P. Li and D. Zhu, *Precis. Eng.*, 47 (2017) 487.
26. S. H. Wang, D. Zhu, Y. B. Zeng and Y. Liu, *Int. J. Adv. Manuf. Technol.*, 53 (2011) 535.

© 2018 The Authors. Published by ESG ([www.electrochemsci.org](http://www.electrochemsci.org)). This article is an open access article distributed under the terms and conditions of the Creative Commons Attribution license (<http://creativecommons.org/licenses/by/4.0/>).